Journal of Pharmaceutical Innovation (2023) 18:1264–1278
https://doi.org/10.1007/s12247-023-09711-y

ORIGINAL ARTICLE

# Nanospanlastics as a Novel Approach for Improving the Oral Delivery of Resveratrol in Lipopolysaccharide-Induced Endotoxicity in Mice

**Mostafa Mohamed Younis**[1] · **Noha Abd El-Fattah Fadel**[2] · **Asmaa Badawy Darwish**[1] · **Amira Mohamed Mohsen**[1]

Accepted: 13 January 2023 / Published online: 4 March 2023


## Abstract

**Purpose** Resveratrol (RSV) is a natural polyphenolic compound that has numerous biological effects. Owing to its poor bioavailability, only trace concentrations of RSV could be found at the site of action. Therefore, the present study was aimed at developing RSV-loaded nanospanlastics to improve its oral delivery and therapeutic activity.

**Methods** RSV-loaded nanospanlastics were prepared using the thin film hydration technique. The developed formulations were characterized via vesicular size (VS), polydispersity index (PDI), zeta potential (ZP) measurements, fourier transform infrared (FT-IR) spectroscopy analysis and transmission electron microscopy (TEM). In vitro release profile was carried out using dialysis bag diffusion technique. In vivo study was carried out using lipopolysaccharide (LPS)-induced endotoxicity model in mice to evaluate the formulations activity.

**Results** The results revealed the successful development of RSV-loaded nanospanlastics which exhibited EE% ranging from 45 to 85%, particle sizes ranging from 260.5 to 794.3 nm; negatively charged zeta potential ($\leq -20$ mV) and TEM revealed their spherical shape. An in vitro release study showed biphasic pattern with sustained release of drug up to 24 h. In vivo results showed the superiority of RSV-loaded nanospanlastics over conventional niosomes in attenuating serum levels of liver and kidney functions (aspartate transaminase (AST), alanine transaminase (ALT), and creatinine) in LPS-induced endotoxic mice. Furthermore, both of them suppressed the elevated oxidative stress and inflammatory markers (malondialdehyde (MDA), nitric oxide (NO), and interleukin-1beta (IL-1β)) estimated in the liver and kidney tissues. However, the nanospanlastics showed a prevalence effect over conventional niosomes in kidney measurements and the histopathological examinations.

**Conclusions** These findings reveal the potential of nanospanlastics in improving the oral delivery and therapeutic efficacy of RSV.

**Keywords** Resveratrol · Nanospanlastics · Niosomes · Lipopolysaccharide · Endotoxicity

## Introduction

Systemic inflammation is considered a hallmark of sepsis that can be provoked by parasites, bacteria, mycobacteria, viruses, and fungus but mainly by gram-negative bacteria [1]. Lipopolysaccharide (LPS) is an endotoxin constituent derived from the cell walls of gram-negative bacteria that harm the host via triggering a systemic inflammatory response with the onset of septic shock and may lead to death [2]. Upon activation of macrophages by LPS, the inflammatory response is initiated by a cascade of mediators including cytokines, mainly interleukins and tumor necrosis factor-α, as well as the production of reactive oxygen species (ROS) and reactive nitrogen species (RNS), followed by alteration of hemostasis that finally led to multiple organ dysfunction [3, 4].

Resveratrol (RSV) is a natural polyphenolic compound formed by plants as a result of abiotic stresses, like ultraviolet (UV) light exposure or existence of heavy metal ions. RSV can be found in grapes, nuts, and blackberries. It is considered a novel nutraceutical, providing consumers with a wide range of health benefits in addition to its basic nutritional value. RSV

✉ Mostafa Mohamed Younis
most_younis@hotmail.com

[1] Pharmaceutical Technology Department, National Research Centre, El-Buhouth Street Dokki, Cairo, Egypt

[2] Drug Radiation Research Department, National Centre for Radiation Research and Technology (NCRRT), Egyptian Atomic Energy Authority, Nasr City, Cairo, Egypt

exhibits geometric isomerism, but trans-resveratrol (trans-3,4,5-trihidroxystilbene) is the only isomer that shows biological activities such as anticancer, anti-inflammatory, antidiabetic, cardioprotective, and antiaging [5]. The protective effect of RSV in the LPS-induced endotoxemia model has been previously reported, as RSV was able to hinder the induced oxidative stress in the brain, liver, and kidney [6–8] and to interfere with the inflammatory signaling cascades in such model [9]. Despite the fact that RSV was therapeutically used in experimental models of inflammation, its limited bioavailability is regarded a limiting factor. Combination therapy was one of the widely investigated methods to overcome bioavailability issues such as combination with bioenhancing agent or low-dose radiation [10–12].

Due to poor bioavailability of RSV, as it exhibits rapid metabolization and excretion, only minute amounts of free RSV (below 5 µg/ml) can be found in systemic circulation after 25 mg oral dose [13, 14]. Also, RSV is poorly water soluble with a log *p* value of 3.1, and according to the European Pharmacopeia, it is considered "practically insoluble in water"[15]. In addition, RSV has a short half-life of about 8–14 min [16]. Hence, there is limitation in the clinical application of RSV, which suggests the development of novel formulations to protect and stabilize RSV from being degraded, improve its water solubility, provide a prolonged release, enhance its bioavailability, and target it to definite sites [17].

It is vital to overcome RSV's poor water solubility and limited bioavailability in order to clinically translate its positive effects. Efforts to increase the efficiency and safety of therapeutic drugs have focused on integrating the medications into a nanocarrier [18, 19]. Nanosized drug delivery systems have established special consideration aiming at reducing the adverse effects and enhancing the drug therapy efficiency [20, 21]. To improve in-vivo delivery of RSV, various nanoparticle (NP)-based formulations have been studied; these studies comprise drug encapsulation into conventional colloidal carriers such as liposomes [22], loading into solid lipid NPs [23], and encapsulation into biodegradable polymeric NPs [24]. Yet, these nanosystems exhibit rigid nature that lacks deformability and flexibility throughout their way across the biological membranes [25]. Thus, more investigations have been recently performed to improve their elasticity in order to increase their permeability through different biological membranes [26].

Nanospanlastics are surfactant-based nanovesicular carriers that were first set up by Kakkar and Kaur [27]. Nonionic surfactants and edge activators are the main constituents of nanospanlastics [15]. They have a good compatibility with biological systems and a low toxicity owing to the inclusion of nonionic surfactants in their structure [28]. Edge activators act by enhancing the permeability and flexibility of the nanocarriers' vesicular membranes through the biological membranes by squeezing through different pores of the biological layers without disruption [29]. Nanospanlastics are biodegradable, nonimmunogenic, and safe deformable nanovesicles. Both hydrophilic and hydrophobic drugs can be delivered via nanospanlastics, where these drugs are enclosed in the inside hydrophilic compartment and the outer lipid layer, respectively [30]. Nanospanlastics differ from conventional niosomes in terms of their structural rigidity. Cholesterol is known to increase the rigidity of the niosomal structure and make the vesicles less elastic [27]. However, the inclusion of an EA in nanospanlastics formulations offers significant flexibility because the size and zeta potential of the formulations can be changed to meet specific requirements using simple and reliable procedures [31]. Moreover, they are more chemically stable than conventional niosomes [32].

Researchers have previously studied spanlastics as a vital drug delivery system via topical route [25, 33]. One of the goals of the present study is to develop RSV-loaded nanospanlastics and investigate spanlastics as an oral drug delivery system. Thereafter, employing the RSV loaded nanospanlastics therapeutically via oral route in LPS-induced endotoxemia model, aiming to improve its anti-inflammatory efficacy.

## Materials and Methods

### Materials

#### Chemicals

Trans-resveratrol (purity ≥ 98%) was purchased from Carl-Roth (Karlsruhe, German). Lipopolysaccharide (LPS from E. coli serotype 055:B5) was procured from Sigma-Aldrich (St. Louis, MO, USA). Sorbitan monostearate (Span 60) and Sorbitan monooleate (Span 80) were procured from Merck (Schuchardt OHG, Germany). Sorbitan monopalmitate (Span 40) and cholesterol were purchased from Sigma-Aldrich (St. Louis, MO, USA). Tween 80 was obtained from Loba Chemie Co. (India). Kits employed for the measurement of aspartate transaminase (AST), alanine transaminase (ALT), malondialdehyde (MDA), and nitric oxide (NO) were obtained from Biodiagnostic (Cairo, Egypt). Enzyme-linked immunosorbent assay (ELISA) kit for the measurement of interleukin-1beta (IL-1β) was purchased Abcam (Cambridge, MA, USA). Other used chemicals were of analytical grade.

#### Animals

Male albino Swiss mice weighing 25–30 g were sourced from the animal breeding facility of the National Centre for Radiation Research and Technology (NCRRT). Animals were acclimatized for at least one week before experiment in the animal facility of NCRRT. They were allowed to feed on laboratory chow and water ad libitum. All animal experiments complied with the Animal Research Reporting of In-Vivo Experiments (ARRIVE) guidelines and were carried

out in accordance with the National Research Council's Guide for the Care and Use of Laboratory Animals (NIH publications No. 8023, revised 1978). The in vivo study was performed according to the guidelines set by the Research Ethics Committee at the NCRRT (permit number: 57 A/ 21).

## Methods

### Preparation of RSV-Loaded Nanospanlastics

Drug-loaded nanospanlastics were developed by the thin film hydration technique [26, 34] employing nonionic surfactants (NIS) such as Span 60 or Span 40 along with cholesterol. Two edge activators (EA), namely, Span 80 or Tween 80, were used at NIS: EA molar ratios of 9:1 or 8:2. Absolute ethanol and chloroform were used in the ratio (1:1 *v*/*v*) as a solvent to dissolve the drug [29]. In brief, one of the selected NIS, with the edge activators, in definite molar ratios, together with 10 mg drug was dissolved in the organic mixture in a round bottom flask [35, 36]. The mixture of solvents was then evaporated under reduced pressure by a rotary evaporator (Rotavapor, Buchi-M/HB-140, Switzerland) to form a thin film on the wall of the flask. This lipid film was then hydrated in 10 ml phosphate buffer pH 7.4, kept at 60 °C, under rotation for 1 h [37]. Conventional niosomes were also prepared for comparison using the same method where the same steps took place but without adding edge activators. The composition of RSV-loaded vesicular systems is shown in Table 1.

## Characterization of RSV-Loaded Nanospanlastics

### Drug Entrapment Assessment

The prepared RSV-loaded nanospanlastics were separated by centrifugation at 8000 rpm at 4 °C for 45 min using cooling centrifuge (Union 32R, Hanil Co., Gyeonggi-do, Republic of Korea). The pellet was then resuspended in 10 ml distilled water till further investigation. Drug amount entrapped in the developed formulation was detected by lysis of 1 ml of resuspended pellet after addition of adequate quantity of ethanol and sonication for 5 min in a bath sonicator. The content of free RSV was then estimated employing a UV–Vis spectrophotometer (Shimadzu UV–Visible spectrophotometer, 2401/PC, Tokyo, Japan) at 305 nm. Drug entrapped amount was calculated, as entrapment efficiency percentage (EE%), in triplicate, according to the following equation [37]:

$$EE\% = \frac{\text{Amount of entrapped drug}}{\text{Total drug added}} \times 100$$

## Determination of Vesicular Size (VS), Polydispersity Index (PDI), and Zeta Potential (ZP) Measurements

VS, PDI, and ZP of the prepared nanospanlastics and conventional niosomes were measured by dynamic light scattering (DLS) using Malvern Instruments (Malvern, UK; Nano ZS). Multimodal mode was employed in all measurements. ZP measurements were determined after injection of the diluted sample into the specified cell. The measurements were done inFig. 4a–c) triplicate.

## In Vitro Release Profiles

Drug release from RSV suspension, as well as from the selected RSV-loaded nanospanlastics and RSV-loaded niosomes, was investigated by dialysis bag diffusion technique employing a shaking water bath (Memmert, SV 1422, Schwabach, Germany). In a cellulose dialysis bag (dialysis tubing cellulose membrane, Sigma Co., USA; Molecular weight cutoff 12,000–14,000), an aliquot of the resuspended RSV-loaded nanospanlastics (equivalent to 2 mg RSV) was

**Table 1** Composition, entrapment efficiency and physicochemical properties of RSV-loaded nanospanlastics/niosomes

| Code | Molar ratio (*w*/*w* %) | | | | | EE (%) ± S.D | VS (nm) ± S.D | PDI | ZP (mV) ± S.D |
|---|---|---|---|---|---|---|---|---|---|
| | Span 60 | Span 40 | Span 80 | Tween 80 | CHOL | | | | |
| F1 | 9 | – | – | 1 | – | 62.63 ± 0.36 | 794.3 ± 97.78 | 0.411 | − 33.1 ± 5.71 |
| F2 | 8 | – | – | 2 | – | 49.4 ± 0.03 | 618.2 ± 73.30 | 0.371 | − 30.5 ± 7.26 |
| F3 | 9 | – | 1 | – | – | 76.31 ± 0.04 | 716.2 ± 74.29 | 0.407 | − 35.8 ± 3.04 |
| F4 | 8 | – | 2 | – | – | 68.96 ± 0.14 | 558.1 ± 77.54 | 0.237 | − 38.9 ± 6.95 |
| F5 | 1 | – | – | – | 1 | 85.03 ± 0.02 | 328.8 ± 58.10 | 0.339 | − 21.3 ± 7.04 |
| F6 | – | 9 | – | 1 | – | 55.42 ± 0.03 | 398.5 ± 70.64 | 0.316 | − 33 ± 4.12 |
| F7 | – | 8 | – | 2 | – | 45.84 ± 0.03 | 357.7 ± 47.29 | 0.304 | − 35.7 ± 6.27 |
| F8 | – | 9 | 1 | – | – | 65.3 ± 0.04 | 361.6 ± 50.14 | 0.355 | − 41.9 ± 6.11 |
| F9 | – | 8 | 2 | – | – | 62.79 ± 0.05 | 289.5 ± 71.90 | 0.432 | − 34.3 ± 7.19 |
| F10 | – | 1 | – | – | 1 | 71.28 ± 0.09 | 260.5 ± 52.17 | 0.388 | − 46.2 ± 3.60 |

Data are expressed as the mean ± S.D. ($n = 3$)

added. Both ends of the bags were sealed. Based on solubility characteristics of resveratrol and to fulfill sink condition, they were placed in a release solution (media) containing 100 ml of phosphate buffer pH 7.4 and 30% ethanol to reach sink condition [38, 39]. The shaking water bath was set at a temperature of 37 ± 0.5 °C and a rotational speed of 100 rpm. At different time intervals (1, 2, 3, 4, 5, 6, 8, and 24 h), samples were withdrawn and substituted with same volumes of fresh medium to maintain sink condition. Drug concentrations were then determined in the withdrawn samples spectrophotometrically at 305 nm. The ratio of RSV released to the total amount in the dialysis bag was used to calculate the cumulative percent of RSV released. All measurements were carried out three times.

In vitro release results were subjected to various mathematical models such as zero-order, first-order, Higuchi, and Peppas to study the release mechanism of RSV from the prepared nanosystems. The linear regression analysis for the release data was assessed by Microsoft Excel Program. The mechanism was determined using the regression coefficient ($R^2$). $R^2$ close to 1 was considered to be the best fit model. The exponent "$n$" was determined for Peppa's model to determine the RSV release mechanism. According to Peppa's theory, if $n \leq 0.43$, the drug is released via a Fickian diffusion mechanism, if $0.43 < n < 0.85$, the mechanism is non-Fickian diffusion, if $n = 0.85$, the mechanism is case II transport, and if $n > 0.85$, the mechanism is super-case II transport [40, 41].

### Fourier Transform Infrared (FT-IR) Spectroscopy Analysis

FT-IR spectroscopy analysis was performed for the selected formulations F8 and F10, along with individual components (RSV, and Span 40) on a JASCO 6100 FT-IR spectrophotometer (JASCO, Tokyo, Japan). Potassium bromide (KBr) was added to the sample first. The mixture was then compacted for 2 min using a hydraulic press at a pressure of 200 kg/cm$^2$. At wavenumbers ranging from 4000 to 400 cm$^{-1}$, a KBr pellet manufactured for each sample was scanned against a KBr blank pellet.

### Transmission Electron Microscopy (TEM)

TEM was performed to determine the morphological characteristics of the selected vesicles [42]. Samples were diluted ten folds with bidistilled water and mixed well prior to the examination. A drop of the investigated formulation was put on a carbon-coated copper grid. Then, it was air-dried at room temperature for 10 min. Afterwards, phosphotungstic acid solution (1% (*w*/*v*)) was dropped to the grid and dried. The grid was then loaded to TEM (JEOL Co., JEM-2100, Tokyo, Japan).

## In Vivo Studies

### Experimental Design

LPS-induced endotoxicity model was carried out in the in-vivo studies to evaluate the anti-inflammatory efficacy of selected RSV formulations. Mice were divided into six groups (n = 6). In Groups I and II, mice received saline and served as negative and positive controls, respectively. In Group III, mice received free RSV (50 mg/kg) suspended in saline [3, 12]. In Groups IV and V, mice received RSV-loaded nanospanlastics (F8) and RSV-loaded niosome (F10) formulations, respectively. The dose of RSV in F8 and F10 formulations is equivalent to that of the free drug group. In Group VI, mice received dexamethasone (DEX; 2 mg/kg) and served as the standard anti-inflammatory drug group [43].

Treatments were orally administered daily for 3 consecutive days except Group VI which was injected intraperitoneally with dexamethasone only once at the third day [3, 9]. After 1 hour from the last treatment dosage, a single dose of LPS (1 mg/kg) was injected intraperitoneally into all animals [44, 45] except for Group I, which served as the normal/negative control group. The current dose of RSV was selected according to the previous study of El-Ghazaly et al. [12] as they postulated that RSV exhibits a submaximal anti-inflammatory effect at such dose level in the carrageenan-induced acute inflammation model.

### Sampling Procedure

At the end of experiment, mice were sacrificed by decapitation under urethane anesthesia, 5 hours post LPS injection. The blood samples were collected, and serum was obtained by cooling centrifugation at 4000 rpm at 4 °C for 10 min and then divided into small aliquots that were stored at − 80 °C for eventual use in estimating liver and kidney functions. Thereafter, livers and kidneys were dissected, washed with saline, and homogenized in ice-cold PBS to prepare 20% homogenates which were centrifuged at 4000 rpm at 4 °C for 10 min. The supernatants were then distributed into several aliquots and stored at − 80 °C to be employed for biochemical tissue analysis. Parts of the livers and kidneys from each group were kept in 10% formalin, to be used for histopathological evaluation.

### Evaluation of Liver and Kidney Functions

The liver and kidney functions (ALT, AST, and creatinine) were measured in serum via a colorimetric method using commercially available kits according to the manufacturer's instructions. The absorbance of each sample was measured using the Unicam 8625 UV/V spectrophotometer (Cambridge, UK).

### Evaluation of Oxidative Stress and Inflammatory Markers

Liver and kidney contents of MDA and NO were estimated by a colorimetric method using commercially available kits, and the absorbance of each sample was measured using a spectrophotometer, while the interleukin-1beta (IL-1β) content was assessed by ELISA using commercially available kit according to the manufacturer's instructions, and ELISA plate reader Dynatec MR5000 (Guernsey, Channel Island, UK) was used to measure the absorbance of each sample.

### Histopathological Evaluation

Tissue specimens of the liver and kidney were fixed in 10% neutral-buffered formalin. They were then trimmed, washed and dehydrated in ascending grades of alcohol, cleared in xylene, and embedded in paraffin blocks. Sections of 5 µm were obtained by sledge microtome and stained with hematoxylin and eosin (H&E) [46]. Images were captured and processed using Adobe Photoshop (version 8). Histopathological examinations were conducted in blind fashion.

### Statistical Analysis

The results were presented as mean values with standard deviations (S.D.). One-way analysis of variance (ANOVA) was used to compare statistical differences between groups, followed by the Tukey–Kramer multiple comparison test. GraphPad prism 5 (Graph Pad Software Inc., San Diego, California, USA) was used for statistical analysis. A $p$ value of less than 0.05 was considered significant. The figures were represented using the Origin® software and the Microsoft Excel programs.

## Results and Discussion

### Preparation of RSV-Loaded Nanospanlastics/Niosomes

RSV-loaded formulations were successfully prepared employing thin film hydration technique and using different nonionic surfactants and edge activators. Table 1 comprises the components and the physicochemical properties of the developed RSV-loaded nanospanlastics/niosomes.

### Characterization of RSV-Loaded Formulations

#### Drug Entrapment Assessment

The EE% of all formulations is illustrated in Table 1, where entrapment efficiencies ranged from $45.84 \pm 0.039$ to $85.03 \pm 0.022$%. The results reflect the effects of nonionic surfactant type (Span 60 and Span 40) and edge activators (Span 80 and Tween 80) on EE% for all prepared formulations. It could be concluded that nanospanlastics prepared using Span 60 showed higher EE% than those prepared using Span 40 at the same molar ratio and same edge activator. This may be attributed to the effect of the surfactant alkyl chain length, which is directly proportional to the EE% [47]. Span 60 has a longer alkyl chain (C16) than Span 40 (C14); this resulted in a higher EE%. Moreover, HLB plays an important role in drug EE%; the higher the HLB of the surfactant, the lower will be the EE%. Since Span 60 HLB (4.7) is smaller than that of Span 40 (6.7), thus, higher EE% was revealed by Span 60 nanospanlastics [37]. The same was revealed, upon comparing EE% of the two conventional niosomes prepared, where Span 60 niosomes (F5) showed higher EE% than Span 40 niosomes (F10).

The formulations F2 and F7 showed the least entrapment efficiencies, i.e., $49.4 \pm 0.033$ and $45.84 \pm 0.039$%, respectively, when compared to other prepared formulations. It can be concluded that increasing the amount of Tween 80 as edge activator led to formation of unstable bilayers, increased leakiness, and permeation of drugs enclosed in the vesicles. Also, inclusion of Tween 80, with high concentrations, reduces the viscosity of the formulation signifying less rigidity of the bilayer membrane. As the presence of unsaturation in Tween 80's alkyl chains increases the bending of the alkyl chains to a degree that can affect the tightness of the developing vesicular membranes, these effects can enhance membrane permeability and increase RSV escape into the external phases [48]. On the other hand, the lack of unsaturation in Span 80's alkyl chains would allow for the construction of more rigid vesicular membranes capable of reducing drug leakage [49]. The edge activator concentration had a beneficial effect on drug EE% until a critical span: edge activator ratio of 4:1, in which lower drug EE % was obtained beyond this ratio [50].

On the opposite side, the edge activator-free dispersions (conventional niosomes F5 and F10), which were prepared using Span 60 or 40 and cholesterol, showed the highest entrapment efficiency ($85.03 \pm 0.022$ and $71.28 \pm 0.093$). These observations reflect the important role of cholesterol which resulted in an increase in the viscosity of the formulation and increased the rigidity and stability of the bilayer membrane, preventing the leakiness and retard permeation of solutes enclosed in the niosomes [51].

#### Vesicular Size (VS), Polydispersity Index (PDI), and Zeta Potential (ZP) Measurements

The mean VS, ZP, and PDI values of the developed dispersions are presented in Table 1. Vesicle sizes of different formulations were in the nanorange between 260.5 and

794.3 nm. It could be depicted that VS of nanospanlastics prepared employing span 60 showed an increased size compared to those prepared using span 40. This increase is related to the increase of Span alkyl chain length, which results in an enhanced critical packing parameter and thus an increase in vesicle size [52]. The results also reveal that smaller particles were formed upon increasing edge activator concentration. This might be attributed to the surfactant ability to reduce interfacial tension. A higher concentration of the edge activator decreased the surface tension, allowing particle partition and produced smaller nanovesicles. Similar results were reported previously [53, 54]. The positive influence of the edge activators on the developed formulations can be observed by their lower aggregation tendency. The PDI is used to determine the size distribution's width. It was previously reported that when PDI values are < 0.5 this indicates homogeneity and narrow distribution [55, 56]. PDI values of the developed formulations ranged from 0.237 to 0.432 revealing that the dispersed particles were homogenously distributed.

The potential stability of the colloidal system can be indicated by the ZP magnitude. It was reported that ZP values >|20| usually indicate minor particle aggregation [57, 58]. ZP values of all the prepared formulations showed highly negative values ranging between − 21.3 mv and − 46.2 mv (Table 1), indicating a good stability. Negative ZP values for vesicles, prepared without adding any charge inducing agents, could be due to preferential adsorption of hydroxyl ions or adsorption of counter ions at the vesicle surface [59] which are sufficiently high for electrostatic stabilization. Due to their highest EE% and suitable VS and ZP, RSV-loaded nanospanlastics F3 and F8 with molar ratio (Span 60 or 40: Span 80; 9:1) and conventional niosomes F5 and F10 of the molar ratios Span 60 or Span 40: Cholesterol (1:1) were selected for further investigations.

## In Vitro Release Study

Drug release from a delivery system is a standard quality control test for verifying consistency of the final product in order to achieve an ideal system with desired release characteristics [60]. Furthermore, vesicular formulations are frequently subjected to in-vitro release experiments in order to anticipate their in vivo performance [61, 62].

Figure 1 demonstrates the release patterns of the investigated nanospanlastics/niosomal formulations. It was observed that the drug release was biphasic, starting with a relatively rapid drug release that lasted for 8 h, with the release of more than 70% of the entrapped RSV in niosomal formulations (F5 and F10). Fast release was followed by a steady phase with a reduced and slow-release rate

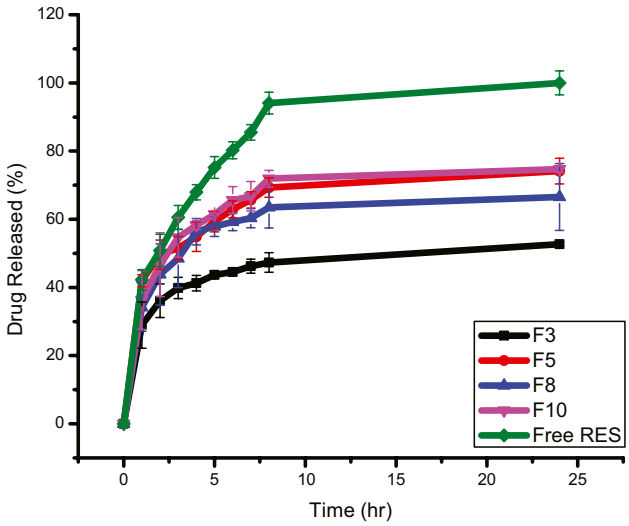


**Fig. 1** Release profiles of RSV from RSV-loaded nanospanlastics and niosomal formulae (F3, F5, F8, and F10) as well as free drug suspension

that was retained for 24 h. The same pattern was observed with the nanospanlastics formulations F3 and F8, as fast release occurred in the first 8 h and about 40% to 60% of the entrapped RSV was released. This was followed by a sustained and slow release that lasted for 24 h. Vesicular sizes played a vital role in drug release, where vesicles with smaller sizes (F5 and F10) showed faster release than those having larger sizes (F3 and F8).

This biphasic release pattern is consistent with previously reported studies and seems to be a common feature of bilayer vesicles [63–65]. The initial rapid to moderate release phase might be attributed to the diffusion of unentrapped drug that may be adsorbed on the surface of the prepared vesicles. The persistent slower release phase is due to RSV progressively diffusing through the bilayers and into the media [66, 67].

The linear regression analysis of the mathematical models used for RSV release data from the selected vesicular formulations revealed that correlation coefficient ($R^2$) values of all formulations were best fitted to Higuchi's model. The Peppas equation was used for further understand of the mechanism of RSV release [40, 68]. Values of the release exponent "*n*" for F3, F5, F8, and F10 were found to be 0.1734, 0.210, 0.195, and 0.2013 respectively (Table 2), indicating a diffusion-controlled release mechanism, i.e., Fickian mechanism. This comes in accordance with previous studies [69–71] where Fickian mechanism was the estimated release mechanism from different vesicular systems. Having optimum drug release and suitable EE%, PS, and ZP and the nanospanlastics F8 and its conventional niosomes F10 were selected for further investigations.

**Table 2** The calculated correlation coefficients and kinetics parameters of RSV release profile from different formulations

| Code | $Q_{8h} \pm$ SD (%) | Zero order | First order | Higuchi | Peppas | |
|---|---|---|---|---|---|---|
| | | $R^2$ | | | $R^2$ | $n$ |
| F3 | 47.32 ± 2.87 | 0.5063 | 0.4345 | 0.68001 | 0.8767 | 0.1734 |
| F5 | 69.30 ± 2.85 | 0.5135 | 0.4595 | 0.68608 | 0.9728 | 0.2100 |
| F8 | 63.48 ± 6.05 | 0.3725 | 0.3131 | 0.538155 | 0.8392 | 0.1959 |
| F10 | 71.92 ± 2.45 | 0.3953 | 0.3319 | 0.565167 | 0.8806 | 0.2013 |
| Free RSV | 85.55 ± 7.68 | 0.5920 | 0.4699 | 0.7571 | 0.9057 | 0.1950 |

$Q_{8h}$ percent total RSV released after 8 h

## Fourier Transform Infrared (FT-IR) Spectroscopy Analysis

FT-IR spectroscopy is a useful tool for finding the principal peaks of a material's unique functional groups and their changes within a specified finger printing region [72]. The interaction of RSV with different components of nanospanlastics and niosomes was studied using FT-IR. The FT-IR spectra of Span 40, RSV, and selected RSV-loaded nanospanlastics and niosomal formulae are shown in Fig. 2. The pursue spectra were achieved at a wavenumber ranging between 4,000 and 650 $cm^{-1}$ [73].

In brief, Span 40 spectrum showed characteristic peaks of 2920 $cm^{-1}$, 2921 $cm^{-1}$, 2926 $cm^{-1}$, and 2929 $cm^{-1}$, which indicate the carboxylic acid functional group. RSV spectrum showed a peak at 3293 $cm^{-1}$ assigned to the vibrations of its free -O–H stretching. It also showed three typical strong absorption bands at 1605 $cm^{-1}$,1583 $cm^{-1}$, and 1380 $cm^{-1}$ corresponding to C–C aromatic double bond stretching, C–C olefinic stretching, and C–C stretching, respectively (benzene skeleton vibrations) [74, 75]. The other peaks obtained at 674, 828, 966, 1147, and 1588 $cm^{-1}$ were attributed to –O–H, –C– –C–H, –C–O, –C–C–, and C– –C bonds of benzene ring, respectively [76].

The IR spectrum of the optimized RSV-loaded nanospanlastics and niosomes (F8 and F10) showed a minor shifting and decreased intensity in the characteristic's peaks of both RSV and different components. The minor changes in the characteristic peaks of RSV might be attributed to the occurrence of physical interaction between RSV and non-ionic surfactant, such as Van der Wall bonds, hydrogen bond, or dipole interactions, with no chemical changes in RSV structure after encapsulation which can lead to optimum entrapment of RSV within nanospanlastics [77]. It is reasonable to believe that RSV's molecular structure has not changed and that it will act normally in encapsulated forms. RSV had been successfully encapsulated, as evidenced by the small changes in intensity [78].

## Transmission Electron Microscopy (TEM)

TEM studies were carried out in order to gain a better understanding of the morphology of the investigated nanospanlastics formulations. Figure 3 demonstrates electron micrographs of different RSV-loaded nanospanlastics and niosomal formulations where the formation of nanospherical vesicles were confirmed by morphological examination of the dispersions.

Vesicles appeared as homogenous, unilamellar, well identified, and almost spherical in shape having definite smooth vesicle surface enclosing an internal aqueous core. The development of closed bilayer vesicles in water may be owing to the amphoteric character of nonionic surfactants (Spans), which causes the hydrophobic part to be oriented away from the aqueous environment while the hydrophilic part kept in touch with

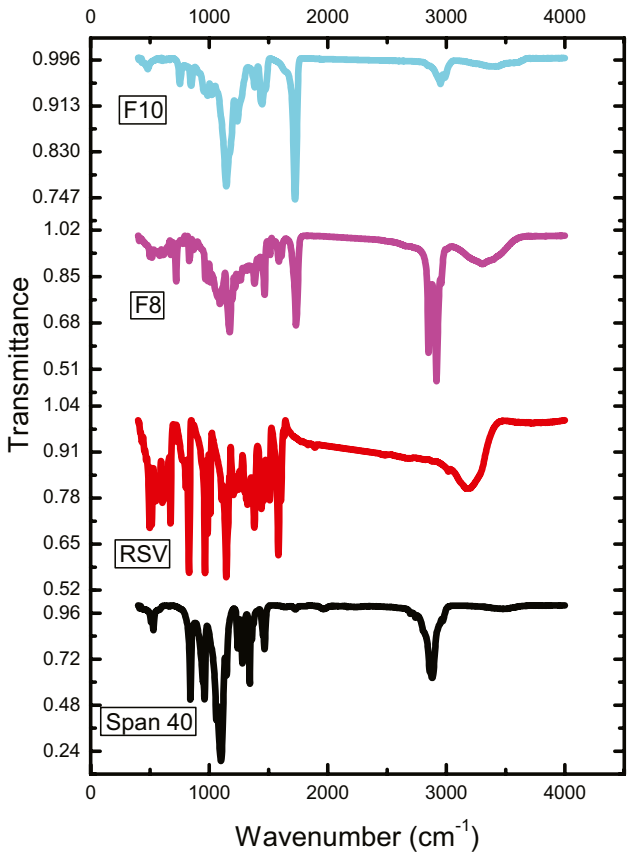


**Fig. 2** FT-IR spectra of free RSV, Span 40 and selected RSV-loaded nanospanlastics and niosomal formulae (F8 and F10)

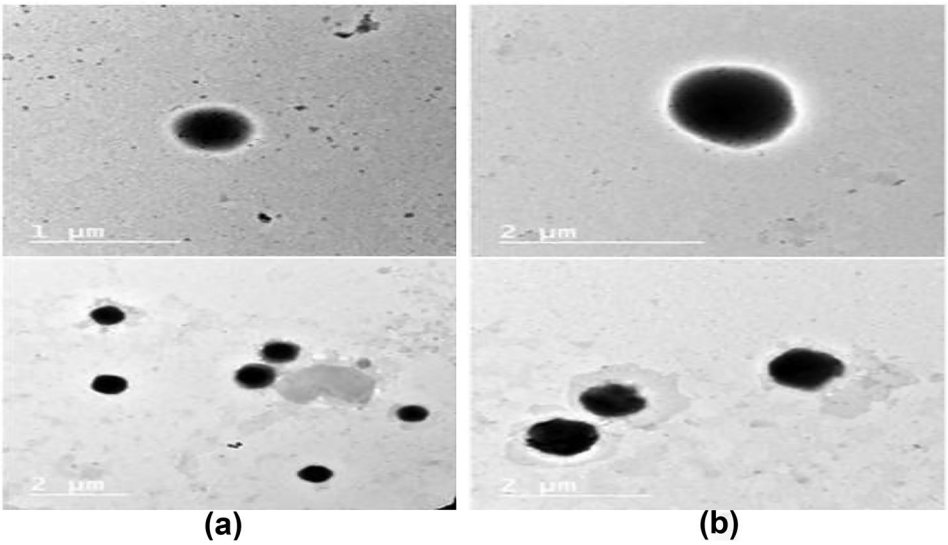


**Fig. 3** TEM of RSV-loaded nanospanlastics and niosomal formulae: **a** F8 and **b** F10

the aqueous environment [79]. To reduce their surface free energy, vesicles must have a tendency to form spherical shapes [80]. The nonaggregated structure of the vesicles could also be linked to the high repulsive interactions between negatively charged surfaces confirmed by ZP results.

## In Vivo Studies

Sepsis-induced multiple organ damage is considered one of the major reasons for morbidity and mortality worldwide. LPS is a potent cytotoxic inducer of inflammation, which lead to pathological syndrome known as endotoxic shock in animals that mimic the septic shock syndrome in humans [81]. Attempts have been done to counteract the deleterious effects associated with sepsis; hence, the current study was constructed in employing the RSV-loaded nanospanlastics via oral route, as a therapeutic strategy in LPS-induced endotoxemia model.

### Assessment of Liver and Kidney Functions

In agreement with previous studies, the data shown in Table 3 revealed that injection of LPS led to a state of liver injury, as shown by the elevated serum transaminases (ALT and AST) activities by 60%, indicating loss of functional integrity and leakage of enzymes typically found in the cytosol into the bloodstream [82]. It was also observed that LPS injection led to a significant increase in the serum creatinine by 80%, as compared to the normal group ($p<0.05$), which reflected the occurrence of kidney damage accompanied with the loss of renal function [83]. Notably, oral administration of free RSV did not show any improvement in the estimated liver and kidney functions, as compared to the LPS group. As for the RSV formulations, oral administration of RSV-loaded nanospanlastics (F8) prior to LPS injection showed a significant decline in the serum levels of the ALT, AST, and creatinine by 22%, 18%, and 24%, respectively. On the other side, pretreatment with F10 significantly suppressed the ALT serum level by 21%, yet it did not induce any significant alteration in the AST and creatinine levels, as compared to the LPS group ($p<0.05$). Interestingly, the efficacy of F8 was similar to a great extent to that of the dexamethasone treated group.

### Assessment of Oxidative Stress and Inflammatory Markers

It has been reported that LPS activates a cascade of signaling pathways that stimulate the release of proinflammatory cytokines which in turn activate migration of neutrophils, macrophages, and dendritic cells. The infiltrated immune

**Table 3** Effect of RSV formulations on the serum levels of ALT, AST, and creatinine, in LPS-induced endotoxicity in mice

| Groups | Parameters | | |
|---|---|---|---|
| | ALT (u/ml) | AST (u/ml) | Creatinine (mg/dl) |
| **Normal** | 61.14 ± 2.688 | 123.60 ± 4.805 | 0.61 ± 0.044 |
| **LPS** | 98.26*± 4.151 | 198.50*± 6.440 | 1.10*± 0.058 |
| **Free RSV/LPS** | 83.16 ± 4.147 | 186.70 ± 4.892 | 0.91 ± 0.072 |
| **F8/LPS** | 77.11$^{\#}$± 5.855 | 161.90$^{\#}$± 4.832 | 0.84$^{\#}$± 0.045 |
| **F10/LPS** | 77.61$^{\#}$± 2.855 | 186.60 ± 6.873 | 1.02 ± 0.055 |
| **DEX/LPS** | 73.14$^{\#}$± 4.742 | 147.30$^{\#}$± 5.022 | 0.70$^{\#}$± 0.063 |

Results are expressed as mean ± S.E. ($n=6$)

*Significantly different ($p<0.05$) compared to the normal group

$^{\#}$Significantly different ($p<0.05$) compared to the LPS group

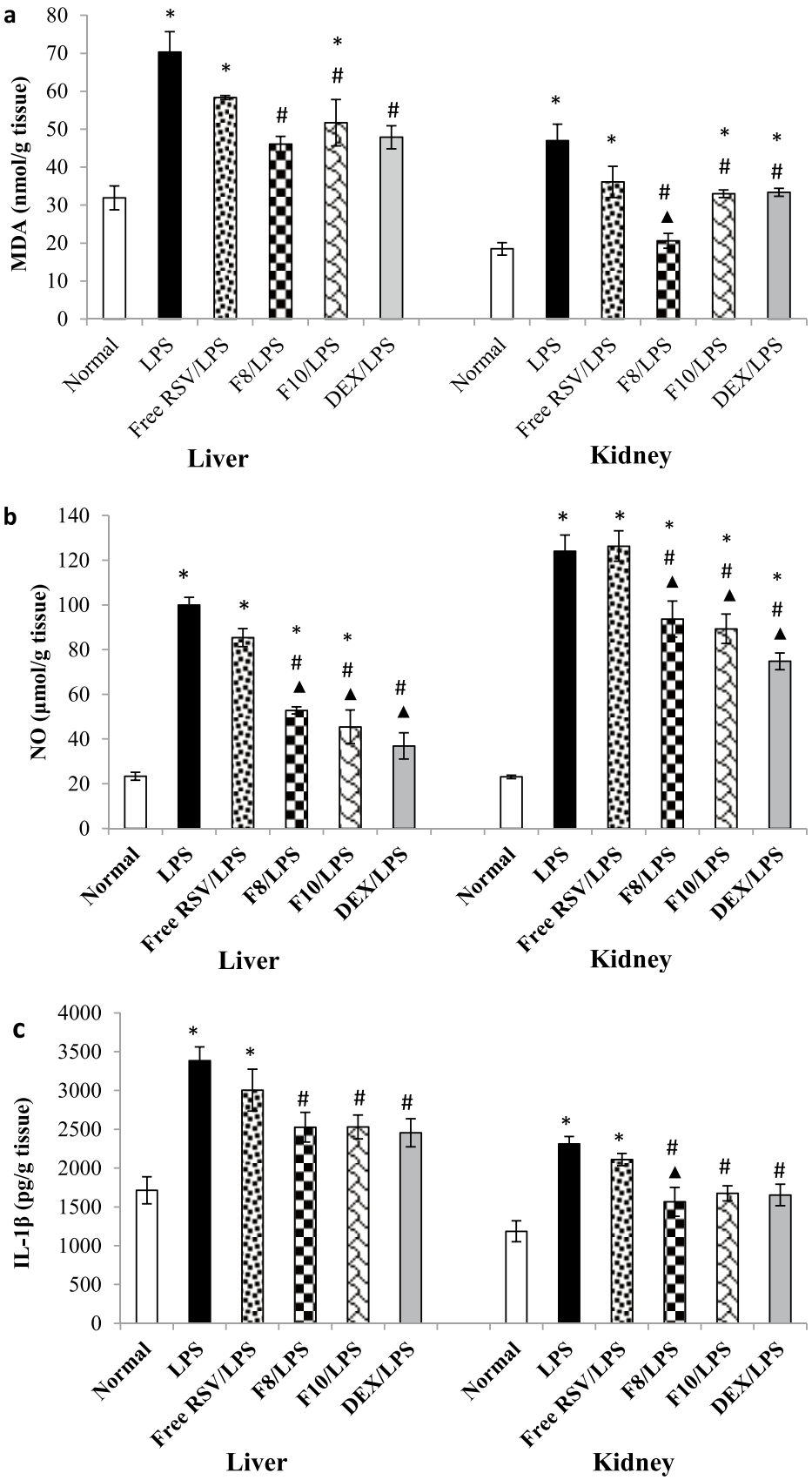


**Fig. 4** Effect of RSV formulations on the liver and kidney contents of **a** MDA, **b** NO, and **c** IL-1β, in LPS-induced endotoxicity in mice. Free RSV (50 mg/kg) and formulations (F8 & F10) were orally administered for 3 consecutive days. LPS (1 mg/kg) was injected intraperitoneally after 1 hour from the last treatment dosage. Results are expressed as the mean ± S.E ($n = 6$). *Significantly different ($p < 0.05$) compared to the normal group; #significantly different ($p < 0.05$) compared to the LPS group; ▲significantly different ($p < 0.05$) compared to the RSV group

cells produce ROS and RNS that led to peroxidation of membrane lipids and subsequently induce a condition of oxidative stress which destroy the surrounding tissues and may contribute to high mortality rates [2]. Hence, the concentrations of MDA (lipid peroxidation product) and NO were estimated in the current study as indicators for the oxidative stress associated with endotoxemia. Among the released cytokine storm, IL-1β concentration was assessed as a major proinflammatory cytokine involved in the inflammatory response induced by LPS challenge [4, 45]. Moreover, IL-1β has been shown to exert a prominent role in the NO synthesis via activation of inducible nitric oxide synthase [84]. Collectively, such cascade was validated in the current study through the elevated concentrations of MDA, NO, and IL-1β, in the liver and kidney tissues of the LPS-challenged group (Fig. 4a–c).

As shown in Fig. 4a–c, oral administration of free RSV did not alter significantly the liver and kidney contents of MDA, NO, and IL-1β, as compared to the LPS group. Indeed, the lack of RSV effect could be attributed to a variety of factors; LPS injection decreased the absorption of RSV owing to the inhibition of RSV transporters [3]. Moreover, the protective effect of RSV in LPS-induced endotoxemia model was demonstrated in the previous studies via intraperitoneal route, where RSV avoids the intestinal metabolism and effectively alleviates the oxidative stress through inhibition of ROS and enhancing the antioxidant enzymes [6, 85, 86]. In addition, the anti-inflammatory efficacy of oral RSV administration in the LPS model was previously correlated with high dose of RSV (100 mg/kg), which is twofold higher than that used in the current study [87].

Regarding the effect of RSV formulations on the assessed liver parameters, oral administration of RSV-loaded spanlastics formula (F8) diminished the elevated liver contents of MDA, NO, and IL-1β by 34%, 47%, and 25%, respectively, as compared to the LPS group ($p < 0.05$). Similarly, pretreatment with conventional niosomes (F10) significantly reduced the previously estimated parameters by 26%, 54%, and 25%, respectively, as compared to the LPS group ($p < 0.05$). Interestingly, the F8 showed prevalence over the F10 in the estimated MDA liver content, where a normalized effect was seen in the F8 treated group ($p < 0.05$) (Fig. 4a–c).

In terms of estimated kidney biomarkers, pretreatment with nanospanlastics formula (F8) suppressed the MDA, NO, and IL-1β concentration by 56%, 24%, and 32%, respectively, as compared to the LPS group ($p < 0.05$), while oral administration of conventional niosomes (F10) repressed the estimated parameters by 30%, 28%, and 28%, respectively, as compared to the LPS group ($p < 0.05$). Remarkably, the nanospanlastics formula (F8) exhibits a significantly enhanced effect than the niosomal formula (F10) in the assessed renal biomarkers, as compared to the free RSV group ($p < 0.05$) (Fig. 4a–c). Notably, the efficacy of nanospanlastics formula (F8) was highly comparable to that of dexamethasone in the previously estimated liver and kidney biomarkers ($p < 0.05$) (Fig. 4a–c).

## Histopathological Examinations

As shown in Fig. 5, hepatic lobules of the normal group had normal architecture, consisting of radiating plates or strands of polygonal cells with conspicuous round nuclei. Sinusoids are lined with a finely arranged layer of Kupffer cells with a discontinuous layer of fenestrated endothelial cells (Fig. 5a). On the other side, hepatic lobules of the LPS group showed hepatic cord disintegration, which appeared as empty vacuoles aligned by necrotic hepatocytes strands. In addition, mononuclear cell infiltration around the necrotic tissues mainly lymphocytes and macrophages with hyperplasia of Kupffer cells was seen (Fig. 5b) that was in line with the previously reported study of Liu et al. [44]. Oral administration of free RSV failed to interfere with such negative consequences, showing moderate to severe degenerative changes that appeared as disorganization of hepatic cords and necrotic alterations in hepatocytes defined by ballooning degeneration and apoptosis of hepatocytes. Nuclear pyknosis and granular cytoplasm of hepatocytes, hepatic sinusoid constriction, and Kupffer cell hyperplasia with mononuclear cell infiltration were observed (Fig. 5c). These deleterious effects were mostly eliminated in the group treated with nanospanlastics formula (F8), showing mild swelling of hepatocytes with hyperplasia of Kupffer cells and decline in the number of inflammatory cells (Fig. 5d). However, treatment with noisome formula (F10) showed moderate hepatocytes degeneration but less severe than the free drug treated group. Hepatic lobules showed focal necrotic areas with mononuclear cell infiltration mainly lymphocytes and macrophages (Fig. 5e). Sections of the dexamethasone treated group showed mild degeneration of hepatic lobules, almost near to that observed in the nanospanlastic-treated group, appeared as hepatocytes swelling, hepatic sinusoid narrowing, and Kupffer cell hyperplasia (Fig. 5f).

Regarding the histopathological examinations of kidney tissues, sections of normal group showed normal architecture of glomerular capillary tufts and Bowman's capsule. The epithelial lining and arrangement of renal tubules were intact (Fig. 6a). On the contrary, sections of LPS group exhibited severe histological changes, showing shrinkage of capillary tufts with widening of Bowman's capsule and swelling of tubular epithelial lining with constriction and occlusion of tubular lumen. Also, necrosis and apoptosis of tubular epithelial cell lining with mononuclear cell infiltration mainly lymphocytes

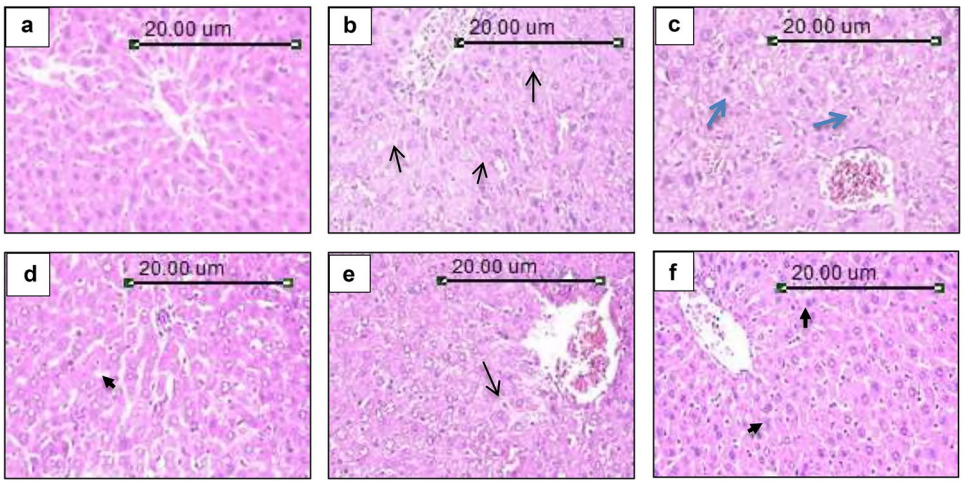


**Fig. 5** Photomicrographs of hepatic tissue sections stained with H&E of **a** normal group, **b** LPS group, **c** free RSV/LPS group, **d** F8/LPS group, **e** F10/LPS group, and **f** dexamethasone/LPS group. Free RSV (50 mg/kg) and formulations (F8 & F10) were orally administered for 3 consecutive days. LPS (1 mg/kg) was injected intraperitoneally after 1 hour from the last treatment dosage. All photomicrographs were taken at magnification power (X200). The following are presented in the tissue sections: necrotic hepatocytes (arrow), swelling of hepatocytes (arrow head), ballooning degeneration, and apoptosis of hepatocytes (blue arrow)

and macrophages were observed (Fig. 6b); such effect was found to be consistent with the findings of a previous investigation [83]. Pretreatment with the free drug had no impact on the developed histological alterations and substantial tissue deterioration was found (Fig. 6c). Furthermore, treatment with nanospanlastics formula (F8) highly alleviates the severity of injury, showing mild histological changes, which appeared in the form of swelling of tubular epithelial lining. In addition, tubular epithelial cell lining degeneration was observed without significant necrosis or apoptosis. The glomeruli have no significant pathological alteration (Fig. 6d). However, pretreatment with noisome formula (F10) partially mitigated the induced injury, in which perivascular edema and mononuclear cell infiltration associated with tubular epithelial cell necrosis and apoptosis was seen, but less severe than the free drug-treated group (Fig. 6e). Mild histological change was observed in the dexamethasone treated groups which was

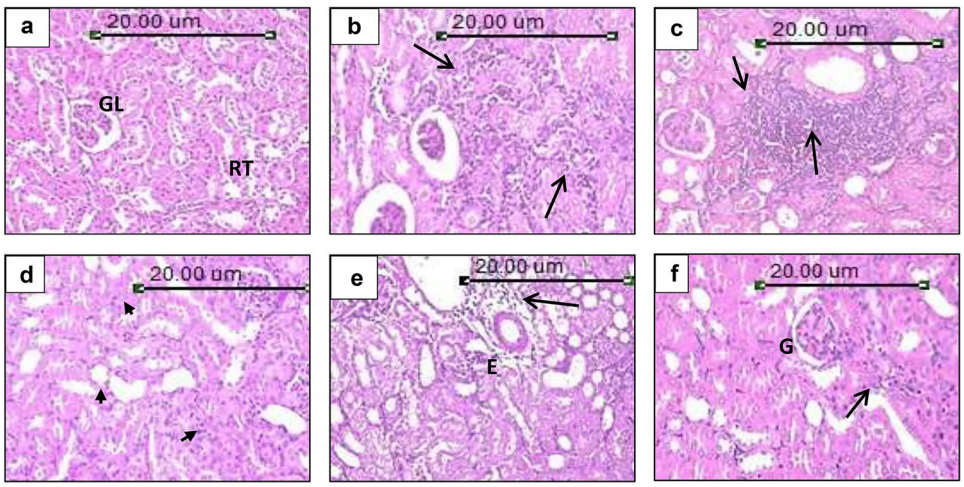


**Fig. 6** Photomicrographs of kidney tissue sections stained with H&E of **a** normal group, **b** LPS group, **c** free RSV/LPS group, **d** F8/LPS group, **e** F10/LPS group, and **f** dexamethasone/LPS group. Free RSV (50 mg/kg) and formulations (F8 & F10) were orally administered for 3 consecutive days. LPS (1 mg/kg) was injected intraperitoneally after 1 hour from the last treatment dosage. All photomicrographs were taken at magnification power (X200). The following are presented in the tissue sections: glomeruli (GL) and renal tubules (RT), inflammatory cell infiltration (arrow), swelling of renal tubule (arrow head), edema (E), and shrinkage of glomeruli (G)

quite comparable to those in the nanospanlastics treated group, showing shrinkage of capillary tufts with widening of Bowman's space of some glomeruli and few numbers of mononuclear cell infiltration (Fig. 6f).

Interestingly, results of the histopathological examinations were in harmony with the biochemical data, revealing the superiority of nanospanlastics in delivering a sufficient concentration of RSV to the circulation and thereby enhancing its therapeutic efficacy.

## Conclusion

In the current investigation, RSV was successfully loaded in nanospanlastics and niosomes prepared with Span 60 or Span40 and EAs (Span 80and tween 80) at two molar ratios of 9:1 and 8:2 for nanospanlastics or Span 60 or Span40 with cholesterol at molar ratio 1:1 for niosomes. All the prepared vesicles were in a nanosize range with high encapsulation efficiency and negatively ZP values. The nanospanlastics formulations F3 and F8 along with niosomal formulations F5 and F10 were chosen for further examination due to its high EE%, suitable VS and ZP values. RSV release from the selected formulations was biphasic and followed a diffusion-controlled release kinetic model. TEM and FT-IR of the selected formulations confirmed the formation of nanospanlastics and niosomes.

Collectively, as shown by the biochemical investigations, F8 showed prevalence effect over free RSV in all the estimated parameters. Although no significant difference was observed between F8 and F10 in the assessed parameters, F8 showed a more prominent effect than F10 in mitigating liver and kidney functions (mainly AST and creatine) and attenuating the inflammatory and oxidative state induced in kidney tissue. Also, F8 exhibits a significant difference from free RSV in the estimated parameters in the kidney tissue. Moreover, the histopathological examinations of liver and kidney tissues showed the efficacy of F8 over free RSV and F10 in alleviating tissue harm. Hence, the current results reported the potential role of nanosapanlastics in enhancing the oral delivery of RSV in experimentally induced endotoxemia, which could be regarded as one of the promising methods for resolving the oral limitation of such a crucial medication.

**Funding** Open access funding provided by The Science, Technology & Innovation Funding Authority (STDF) in cooperation with The Egyptian Knowledge Bank (EKB). Project's Sector at the National Research Centre, Cairo, Egypt E120201.



## References

1. Annane D, Bellissant E, Cavaillon JM. Septic shock. Lancet. 2005;365(9453):63–78. https://doi.org/10.1016/s0140-6736(04)17667-8.
2. Rietschel ET, Kirikae T, Schade FU, Mamat U, Schmidt G, Loppnow H, et al. Bacterial endotoxin: molecular relationships of structure to activity and function. FASEB J. 1994;8(2):217–25. https://doi.org/10.1096/fasebj.8.2.8119492.
3. Larrosa M, Azorín-Ortuño M, Yañez-Gascón MJ, García-Conesa MT, Tomás-Barberán F, Espín JC. Lack of effect of oral administration of resveratrol in LPS-induced systemic inflammation. Eur J Nutr. 2011;50(8):673–80. https://doi.org/10.1007/s00394-011-0178-3.
4. Kolac UK, Ustuner MC, Tekin N, Ustuner D, Colak E, Entok E. The anti-inflammatory and antioxidant effects of Salvia officinalis on lipopolysaccharide-induced inflammation in rats. J Med Food. 2017;20(12):1193–200. https://doi.org/10.1089/jmf.2017.0035.
5. Rauf A, Imran M, Suleria HaR, Ahmad B, Peters DG, Mubarak MS. A comprehensive review of the health perspectives of resveratrol. Food Funct. 2017;8(12):4284–305. https://doi.org/10.1039/c7fo01300k.
6. Sebai H, Gadacha W, Sani M, Aouani E, Ghanem-Boughanmi N, Ben-Attia M. Protective effect of resveratrol against lipopolysaccharide-induced oxidative stress in rat brain. Brain Inj. 2009;23(13–14):1089–94. https://doi.org/10.3109/02699050903379370.
7. Sebai H, Sani M, Yacoubi MT, Aouani E, Ghanem-Boughanmi N, Ben-Attia M. Resveratrol, a red wine polyphenol, attenuates lipopolysaccharide-induced oxidative stress in rat liver. Ecotoxicol Environ Saf. 2010;73(5):1078–83. https://doi.org/10.1016/j.ecoenv.2009.12.031.
8. Sebai H, Ben-Attia M, Sani M, Aouani E, Ghanem-Boughanmi N. Protective effect of resveratrol on acute endotoxemia-induced nephrotoxicity in rat through nitric oxide independent mechanism. Free Radic Res. 2008;42(11–12):913–20. https://doi.org/10.1080/10715760802555577.
9. Wang G, Hu Z, Fu Q, Song X, Cui Q, Jia R, et al. Resveratrol mitigates lipopolysaccharide-mediated acute inflammation in rats by inhibiting the TLR4/NF-κBp65/MAPKs signaling cascade. Sci Rep. 2017;745006. https://doi.org/10.1038/srep45006.
10. El-Ghazaly MA, Fadel NA, Abdel-Naby DH, Abd El-Rehim HA, Zaki HF, Kenawy SA. Amelioration of adjuvant-induced arthritis by exposure to low dose gamma radiation and resveratrol administration in rats. Int J Radiat Biol. 2020;96(7):857–67. https://doi.org/10.1080/09553002.2020.1748911.
11. Penalva R, Esparza I, Larraneta E, González-Navarro CJ, Gamazo C, Irache JM. Zein-based nanoparticles improve the oral bioavailability of resveratrol and its anti-inflammatory effects in a mouse model of endotoxic shock. J Agric Food Chem. 2015;63(23):5603–11. https://doi.org/10.1021/jf505694e.
12. El-Ghazaly MA, Fadel NA, Abdel-Naby DH, Abd El-Rehim HA, Zaki HF, Kenawy SA. Potential anti-inflammatory action of resveratrol and piperine in adjuvant-induced arthritis: effect on pro-inflammatory cytokines and oxidative stress biomarkers.

Egypt Rheumatol. 2020;42(1):71–7. https://doi.org/10.1016/j.ejr.2019.08.003.
13. Walle T. Bioavailability of resveratrol. Ann N Y Acad Sci. 2011;12159–15. https://doi.org/10.1111/j.1749-6632.2010.05842.x.
14. Walle T, Hsieh F, Delegge MH, Oatis JE, Jr., Walle UK. High absorption but very low bioavailability of oral resveratrol in humans. Drug Metab Dispos. 2004;32(12):1377–82. https://doi.org/10.1124/dmd.104.000885.
15. Pace-Asciak CR, Hahn S, Diamandis EP, Soleas G, Goldberg DM. The red wine phenolics trans-resveratrol and quercetin block human platelet aggregation and eicosanoid synthesis: implications for protection against coronary heart disease. Clin Chim Acta. 1995;235(2):207–19. https://doi.org/10.1016/0009-8981(95)06045-1.
16. Baur JA, Sinclair DA. Therapeutic potential of resveratrol: the in vivo evidence. Nat Rev Drug Discov. 2006;5(6):493–506. https://doi.org/10.1038/nrd2060.
17. Kalita B, Das MK, Sarma M, Deka A. Sustained anti-inflammatory effect of resveratrol-phospholipid complex embedded polymeric patch. AAPS PharmSciTech. 2017;18(3):629–45. https://doi.org/10.1208/s12249-016-0542-y.
18. Kesharwani P, Gorain B, Low SY, Tan SA, Ling ECS, Lim YK, et al. Nanotechnology based approaches for anti-diabetic drugs delivery. Diabetes Res Clin Pract. 2018;13652–77. https://doi.org/10.1016/j.diabres.2017.11.018.
19. Mohsen AM. Nanotechnology advanced strategies for the management of diabetes mellitus. Curr Drug Targets. 2019;20(10):995–1007. https://doi.org/10.2174/1389450120666190307101642.
20. Alonso MJ. Nanomedicines for overcoming biological barriers. Biomed Pharmacother. 2004;58(3):168–72. https://doi.org/10.1016/j.biopha.2004.01.007.
21. Elmeshad AN, Mohsen AM. Enhanced corneal permeation and antimycotic activity of itraconazole against Candida albicans via a novel nanosystem vesicle. Drug Deliv. 2016;23(7):2115–23. https://doi.org/10.3109/10717544.2014.942811.
22. Coimbra M, Isacchi B, Van Bloois L, Torano JS, Ket A, Wu X, et al. Improving solubility and chemical stability of natural compounds for medicinal use by incorporation into liposomes. Int J Pharm. 2011;416(2):433–42. https://doi.org/10.1016/j.ijpharm.2011.01.056.
23. Neves AR, Lúcio M, Martins S, Lima JL, Reis S. Novel resveratrol nanodelivery systems based on lipid nanoparticles to enhance its oral bioavailability. Int J Nanomedicine. 2013;8177–87. https://doi.org/10.2147/ijn.S37840.
24. Shao J, Li X, Lu X, Jiang C, Hu Y, Li Q, et al. Enhanced growth inhibition effect of resveratrol incorporated into biodegradable nanoparticles against glioma cells is mediated by the induction of intracellular reactive oxygen species levels. Colloids Surf B Biointerfaces. 2009;72(1):40–7. https://doi.org/10.1016/j.colsurfb.2009.03.010.
25. Badria F, Mazyed E. Formulation of nanospanlastics as a promising approach for improving the topical delivery of a natural leukotriene inhibitor (3-acetyl-11-keto-β-boswellic acid): statistical optimization, in vitro characterization, and ex vivo permeation study. Drug Des Devel Ther. 2020;143697–721. https://doi.org/10.2147/dddt.S265167.
26. Al-Mahallawi AM, Khowessah OM, Shoukri RA. Enhanced non invasive trans-tympanic delivery of ciprofloxacin through encapsulation into nano-spanlastic vesicles: fabrication, in-vitro characterization, and comparative ex-vivo permeation studies. Int J Pharm. 2017;522(1–2):157–64. https://doi.org/10.1016/j.ijpharm.2017.03.005.
27. Kakkar S, Kaur IP. Spanlastics--a novel nanovesicular carrier system for ocular delivery. Int J Pharm. 2011;413(1–2):202–10. https://doi.org/10.1016/j.ijpharm.2011.04.027.
28. Sharma A, Pahwa S, Bhati S, Kudeshia P. Spanlastics: a modern approach for nanovesicular drug delivery system. Int J Pharm Sci Res. 2020;11(3):1057–65. https://doi.org/10.13040/IJPSR.0975-8232.
29. Zheng WS, Fang XQ, Wang LL, Zhang YJ. Preparation and quality assessment of itraconazole transfersomes. Int J Pharm. 2012;436(1–2):291–8. https://doi.org/10.1016/j.ijpharm.2012.07.003.
30. De Vries T, Villalon CM, Maassenvandenbrink A. Pharmacological treatment of migraine: CGRP and 5-HT beyond the triptans. Pharmacol Ther. 2020;211107528
31. Abdelbari MA, El-Mancy SS, Elshafeey AH, Abdelbary AA. Implementing spanlastics for improving the ocular delivery of clotrimazole: in vitro characterization, ex vivo permeability, microbiological assessment and in vivo safety study. Int J Nanomedicine. 2021;166249–61. https://doi.org/10.2147/ijn.S319348.
32. Kamboj S, Saini V, Maggon N, Bala S, Jhawat V. Vesicular drug delivery systems: a novel approach for drug targeting. 2013;5(2):121–30.
33. Shaaban M, Nasr M, Tawfik AA, Fadel M, Sammour O. Novel bergamot oil nanospanlastics combined with PUVB therapy as a clinically translatable approach for vitiligo treatment. Drug Deliv Transl Res. 2019;9(6):1106–16. https://doi.org/10.1007/s13346-019-00653-y.
34. Abdelbary G. Ocular ciprofloxacin hydrochloride mucoadhesive chitosan-coated liposomes. Pharm Dev Technol. 2011;16(1):44–56. https://doi.org/10.3109/10837450903479988.
35. Uchegbu IF, Vyas SP. Non-ionic surfactant based vesicles (niosomes) in drug delivery. Int J Pharm. 1998;172(1–2):33–70.
36. Jigar V, Puja V, Krutika S. Formulation and evaluation of topical niosomal gel of erythromycin. Int J Pharm Pharm Sci. 2011;3(1):123–6.
37. Mohsen AM, Abousamra MM, Elshebiney SA. Enhanced oral bioavailability and sustained delivery of glimepiride via niosomal encapsulation: in-vitro characterization and in-vivo evaluation. Drug Dev Ind Pharm. 2017;43(8):1254–64. https://doi.org/10.1080/03639045.2017.1310224.
38. Khalil RM, Abd-Elbary A, Kassem MA, El Ridy MS, Samra M, Awad G, et al. Formulation and characterization of nystatin-loaded nanostructured lipid carriers for topical delivery against cutaneous candidiasis. Br J Pharm Res. 2014;4(4):490–512.
39. Kikwai L, Babu RJ, Prado R, Kolot A, Armstrong CA, Ansel JC, et al. In vitro and in vivo evaluation of topical formulations of spantide II. AAPS PharmSciTech. 2005;6(4):E565–72. https://doi.org/10.1208/pt060471.
40. Peppas NA, Sahlin JJ. A simple equation for the description of solute release. III. Coupling of diffusion and relaxation. Int J Pharm. 1989;57(2):169–72
41. Mohsen AM, Younis MM, Salama A, Darwish AB. Cubosomes as a potential oral drug delivery system for enhancing the hepatoprotective effect of coenzyme Q10. J Pharm Sci. 2021;110(7):2677–86. https://doi.org/10.1016/j.xphs.2021.02.007.
42. El-Ridy MS, Yehia SA, Mohsen AM, El-Awdan SA, Darwish AB. Formulation of niosomal gel for enhanced transdermal lornoxicam delivery: in-vitro and in-vivo evaluation. Curr Drug Deliv. 2018;15(1):122–33. https://doi.org/10.2174/1567201814666170224141548.
43. Soliman MG, Mansour HA, Hassan WA, El-Sayed RA, Hassaan NA. Mesenchymal stem cells therapeutic potential alleviate lipopolysaccharide-induced acute lung injury in rat model. J Biochem Mol Toxicol. 2018;32(11):e22217. https://doi.org/10.1002/jbt.22217.
44. Liu L, Mu Q, Li W, Xing W, Zhang H, Fan T, et al. Isofraxidin protects mice from LPS challenge by inhibiting pro-inflammatory cytokines and alleviating histopathological changes. Immunobiology. 2015;220(3):406–13. https://doi.org/10.1016/j.imbio.2014.10.007.
45. Gao LN, Cui YL, Wang QS, Wang SX. Amelioration of Danhong injection on the lipopolysaccharide-stimulated systemic acute

inflammatory reaction via multi-target strategy. J Ethnopharmacol. 2013;149(3):772–82. https://doi.org/10.1016/j.jep.2013.07.039.
46. Bancroft JD, Stevens A, Turner DR. Theory and practice of histological techniques. New York Churchill Livingstone. 1996.
47. Yoshioka T, Sternberg B, Florence AT. Preparation and properties of vesicles (niosomes) of sorbitan monoesters (Span 20, 40, 60 and 80) and a sorbitan triester (Span 85). Int J Pharm. 1994;105(1):1–6.
48. Tayel SA, El-Nabarawi MA, Tadros MI, Abd-Elsalam WH. Duodenum-triggered delivery of pravastatin sodium via enteric surface-coated nanovesicular spanlastic dispersions: development, characterization and pharmacokinetic assessments. Int J Pharm. 2015;483(1–2):77–88. https://doi.org/10.1016/j.ijpharm.2015.02.012.
49. Hao Y, Zhao F, Li N, Yang Y, Li K. Studies on a high encapsulation of colchicine by a niosome system. Int J Pharm. 2002;244(1–2):73–80. https://doi.org/10.1016/s0378-5173(02)00301-0.
50. Van Den Bergh BA, Wertz PW, Junginger HE, Bouwstra JA. Elasticity of vesicles assessed by electron spin resonance, electron microscopy and extrusion measurements. Int J Pharm. 2001;217(1–2):13–24. https://doi.org/10.1016/s0378-5173(01)00576-2.
51. Abdelbary G, El-Gendy N. Niosome-encapsulated gentamicin for ophthalmic controlled delivery. AAPS PharmSciTech. 2008;9(3):740–7. https://doi.org/10.1208/s12249-008-9105-1.
52. Uchegbu IF, Florence AT. Non-ionic surfactant vesicles (niosomes): physical and pharmaceutical chemistry. Adv Colloid Interface Sci. 1995;58(1):1–55.
53. Dora CP, Singh SK, Kumar S, Datusalia AK, Deep A. Development and characterization of nanoparticles of glibenclamide by solvent displacement method. Acta Pol Pharm. 2010;67(3):283–90.
54. Almuqbil RM, Sreeharsha N, Nair AB. Formulation-by-design of efinaconazole spanlastic nanovesicles for transungual delivery using statistical risk management and multivariate analytical techniques. Pharmaceutics. 2022;14(7):1419.
55. El-Hadi Aa, Ahmed Hm, Zaki Ra, Mohsen Am. Enhance enzymatic activity of streptomyces griseoplanus L-asparginase via its incorporation in an oil-based nanocarrier. Int J App Pharm. 2020203–10. https://doi.org/10.22159/ijap.2020v12i5.38360.
56. Parveen R, Baboota S, Ali J, Ahuja A, Vasudev SS, Ahmad S. Oil based nanocarrier for improved oral delivery of silymarin: in vitro and in vivo studies. Int J Pharm. 2011;413(1–2):245–53. https://doi.org/10.1016/j.ijpharm.2011.04.041.
57. Aditya NP, Shim M, Lee I, Lee Y, Im MH, Ko S. Curcumin and genistein coloaded nanostructured lipid carriers: in vitro digestion and antiprostate cancer activity. J Agric Food Chem. 2013;61(8):1878–83. https://doi.org/10.1021/jf305143k.
58. Mohsen AM. Cationic polymeric nanoparticles for improved ocular delivery and antimycotic activity of Terconazole. J Pharm Sci. 2022;111(2):458–68. https://doi.org/10.1016/j.xphs.2021.09.019.
59. Junyaprasert VB, Teeranachaideekul V, Supaperm T. Effect of charged and non-ionic membrane additives on physicochemical properties and stability of niosomes. AAPS PharmSciTech. 2008;9(3):851–9. https://doi.org/10.1208/s12249-008-9121-1.
60. Joshi M, Patravale V. Nanostructured lipid carrier (NLC) based gel of celecoxib. Int J Pharm. 2008;346(1–2):124–32. https://doi.org/10.1016/j.ijpharm.2007.05.060.
61. Varshosaz J, Pardakhty A, Hajhashemi VI, Najafabadi AR. Development and physical characterization of sorbitan monoester niosomes for insulin oral delivery. Drug Deliv. 2003;10(4):251–62. https://doi.org/10.1080/drd_10_4_251.
62. Hady MA, Darwish AB, Abdel-Aziz MS, Sayed OM. Design of transfersomal nanocarriers of nystatin for combating vulvovaginal candidiasis; a different prospective. Colloids Surf B Biointerfaces. 2021;211112304. https://doi.org/10.1016/j.colsurfb.2021.112304.
63. Hong M, Zhu S, Jiang Y, Tang G, Pei Y. Efficient tumor targeting of hydroxycamptothecin loaded PEGylated niosomes modified with transferrin. J Control Release. 2009;133(2):96–102. https://doi.org/10.1016/j.jconrel.2008.09.005.
64. Barakat HS, Darwish IA, El-Khordagui LK, Khalafallah NM. Development of naftifine hydrochloride alcohol-free niosome gel. Drug Dev Ind Pharm. 2009;35(5):631–7. https://doi.org/10.1080/03639040802498864.
65. Khazaeli P, Pardakhty A, Shoorabi H. Caffeine-loaded niosomes: characterization and in vitro release studies. Drug Deliv. 2007;14(7):447–52. https://doi.org/10.1080/10717540701603597.
66. Azeem A, Anwer MK, Talegaonkar S. Niosomes in sustained and targeted drug delivery: some recent advances. J Drug Target. 2009;17(9):671–89. https://doi.org/10.3109/10611860903079454.
67. Mokhtar M, Sammour OA, Hammad MA, Megrab NA. Effect of some formulation parameters on flurbiprofen encapsulation and release rates of niosomes prepared from proniosomes. Int J Pharm. 2008;361(1–2):104–11. https://doi.org/10.1016/j.ijpharm.2008.05.031.
68. Lokhande AB, Mishra S, Kulkarni RD, Naik JB. Preparation and characterization of repaglinide loaded ethylcellulose nanoparticles by solvent diffusion technique using high pressure homogenizer. J Pharm Res. 2013;7(5):421–6. https://doi.org/10.1016/j.jopr.2013.04.049.
69. Mohsen AM, Salama A, Kassem AA. Development of acetazolamide loaded bilosomes for improved ocular delivery: preparation, characterization and in vivo evaluation. J Drug Deliv Sci Technol. 2020;59101910
70. Allam A, Fetih G. Sublingual fast dissolving niosomal films for enhanced bioavailability and prolonged effect of metoprolol tartrate. Drug Des Devel Ther. 2016;102421–33. https://doi.org/10.2147/dddt.S113775.
71. Khalil RM, Abdelbary A, Kocova El-Arini S, Basha M, El-Hashemy HA. Evaluation of bilosomes as nanocarriers for transdermal delivery of tizanidine hydrochloride: in vitro and ex vivo optimization. J Liposome Res. 2019;29(2):171–82. https://doi.org/10.1080/08982104.2018.1524482.
72. Yeo LK, Olusanya TOB, Chaw CS, Elkordy AA. Brief effect of a small hydrophobic drug (cinnarizine) on the physicochemical characterisation of niosomes produced by thin-film hydration and microfluidic methods. Pharmaceutics. 2018;10(4). https://doi.org/10.3390/pharmaceutics10040185.
73. Abou Taleb S, Darwish AB, Abood A, Mohamed AM. Investigation of a new horizon antifungal activity with enhancing the antimicrobial efficacy of ciprofloxacin and its binary mixture via their encapsulation in nanoassemblies: in vitro and in vivo evaluation. Drug Dev Res. 2020;81(3):374–88. https://doi.org/10.1002/ddr.21632.
74. Kumpugdee-Vollrath M. Solid state characterization of trans resveratrol complexes with different cyclodextrins. J Asian. 2012;1125–36
75. Nishihira VSK, Da Silva Fernandes L, Mortari SR, Raffin RP, Rech VC. Characterization of resveratrol/hydroxipropyl-β-cyclodextrin inclusion complex for subsequent application in hyperglicemic rats. Disciplinarum Sciential Naturais e Tecnológicas. 2013;14(1):67–72
76. Venuti V, Cannavà C, Cristiano MC, Fresta M, Majolino D, Paolino D, et al. A characterization study of resveratrol/sulfobutyl ether-β-cyclodextrin inclusion complex and in vitro anticancer activity. Colloids Surf B Biointerfaces. 2014;11522–8. https://doi.org/10.1016/j.colsurfb.2013.11.025.
77. Mazyed EA, Zakaria S. Enhancement of dissolution characteristics of clopidogrel bisulphate by proniosomes. Int J Appl Pharm. 2019;11(2):77–85. https://doi.org/10.22159/ijap.2019v11i2.30575.
78. Shruthi PA, Pushpadass HA, Franklin MEE, Battula SN, Laxmana Naik N. Resveratrol-loaded proniosomes: formulation, characterization and fortification. LWT. 2020;134(14):110127. https://doi.org/10.1016/j.lwt.2020.110127.
79. Kazi KM, Mandal AS, Biswas N, Guha A, Chatterjee S, Behera M, et al. Niosome: a future of targeted drug delivery systems. J Adv Pharm Technol Res. 2010;1(4):374–80. https://doi.org/10.4103/0110-5558.76435.

80. Das MK, Palei NN. Sorbitan ester niosomes for topical delivery of rofecoxib. Indian J Exp Biol. 2011;49(6):438–45.
81. Poli-De-Figueiredo LF, Garrido AG, Nakagawa N, Sannomiya P. Experimental models of sepsis and their clinical relevance. Shock. 2008;30 Suppl 153–9. https://doi.org/10.1097/SHK.0b013e318181a343.
82. El-Tanbouly DM, Abdelsalam RM, Attia AS, Abdel-Aziz MT. Pretreatment with magnesium ameliorates lipopolysaccharide-induced liver injury in mice. Pharmacol Rep. 2015;67(5):914–20. https://doi.org/10.1016/j.pharep.2015.02.004.
83. Mohamed AF, Safar MM, Zaki HF, Sayed HM. Telluric acid ameliorates endotoxemic kidney injury in mice: involvement of TLR4, Nrf2, and PI3K/Akt signaling pathways. Inflammation. 2017;40(5):1742–52. https://doi.org/10.1007/s10753-017-0617-2.
84. Dinarello CA. The IL-1 family and inflammatory diseases. Clin Exp Rheumatol. 2002;20(5 Suppl 27):S1-13.
85. Chen YY, Zhang L, Shi DL, Song XH, Shen YL, Zheng MZ, et al. Resveratrol attenuates subacute systemic inflammation-induced spatial memory impairment via inhibition of astrocyte activation and enhancement of ynaptophysin expression in the hippocampus. Ann Clin Lab Sci. 2017;47(1):17–24.
86. Sebai H, Ben-Attia M, Sani M, Aouani E, Ghanem-Boughanmi N. Protective effect of resveratrol in endotoxemia-induced acute phase response in rats. Arch Toxicol. 2009;83(4):335–40. https://doi.org/10.1007/s00204-008-0348-0.
87. Chen L, Yang S, Zumbrun EE, Guan H, Nagarkatti PS, Nagarkatti M. Resveratrol attenuates lipopolysaccharide-induced acute kidney injury by suppressing inflammation driven by macrophages. Mol Nutr Food Res. 2015;59(5):853–64. https://doi.org/10.1002/mnfr.201400819.